British Journal of Physics Studies
ISSN: 2755-3388
DOI: 10.32996/bjps
Journal Homepage: www.al-kindipublisher.com/index.php/bjps

BJPS
AL-KINDI CENTER FOR RESEARCH AND DEVELOPMENT

| RESEARCH ARTICLE

Physics-Informed Machine Learning for Porosity Prediction in Laser Powder Bed Fusion of Critical Mechanical Components

Thomas K. Tirado[1], Charlene R. Williams[2], Sheila J. Burditt[3], and Andrea J. Walters[4]
[1234] Department of Mechanical Engineering, University of New Hampshire, Durham, NH 03824, USA
Corresponding Author: Thomas K. Tirado, **E-mail**: Thomas.Tirado@unh.edu

| ABSTRACT

Porosity remains one of the most consequential defects in laser powder bed fusion (LPBF) because even small internal voids can degrade fatigue resistance, fracture performance, leak-tightness, and long-term reliability in safety-critical mechanical components. Purely empirical machine-learning models have shown promise for defect detection, yet they often depend heavily on machine-specific datasets and can lose interpretability outside the training domain. This manuscript develops a physics-informed machine-learning (PIML) framework for porosity prediction in LPBF by integrating process parameters, in-situ monitoring signals, and physically meaningful descriptors such as line energy, volumetric energy density, scan-overlap ratio, Peclet number, cooling-rate proxy, and mechanism-sensitive indicators for lack-of-fusion and keyhole instability. A hybrid learning objective is formulated to combine statistical prediction accuracy with soft physics penalties that discourage mechanistically inconsistent outputs. The paper further proposes a risk-based decision logic suitable for critical-component qualification, where predicted porosity must be interpreted together with uncertainty, part zoning, and inspection requirements. An analytical demonstration is included to show how the framework distinguishes stable, lack-of-fusion-prone, and keyhole-prone process windows. The contribution of the study is therefore methodological: it offers a publication-ready formulation that connects LPBF process physics, monitoring, and machine learning in a single, interpretable workflow that can later be validated with computed tomography, metallography, and mechanical testing data.

| KEYWORDS

laser powder bed fusion; porosity prediction; physics-informed machine learning; critical mechanical components; in-situ monitoring; additive manufacturing

| ARTICLE INFORMATION

ACCEPTED: 27 April 2026 **PUBLISHED:** 03 June 2026 **DOI:** 10.32996/bjps.2026.4.1.1

1. Introduction

Laser powder bed fusion has become one of the most important metal additive manufacturing routes for producing geometrically complex, lightweight, and high-value components used in aerospace, biomedical, tooling, energy, and advanced mechanical systems. Its industrial relevance comes from the ability to manufacture internal channels, near-net-shape geometries, topology-optimized structures, and application-specific features that would be difficult or impossible to fabricate economically through conventional subtractive or formative processes. At the same time, LPBF operates within a narrow process window in which laser energy input, scan speed, hatch spacing, layer thickness, powder quality, and local thermal history interact over very short temporal and spatial scales, making process stability a persistent challenge. Among LPBF defects, porosity remains especially critical. Internal pores may originate from lack of fusion, keyhole instability, gas entrapment, powder contamination, or spatter-related disturbances, and their effect is often disproportionate to their size because pores can act as stress concentrators under cyclic or multiaxial loading. For brackets, manifolds, heat exchangers, pressure-retaining structures, implants, and rotating hardware, subsurface pores can reduce fatigue strength and compromise service reliability even when dimensional inspection is

otherwise satisfactory (Zhao et al., 2017; Huang et al., 2022; Aydogan & Chou, 2024; Chua et al., 2024). This concern is also relevant for thermally demanding additively manufactured heat-transfer hardware, where internal integrity directly affects both performance and safety (Hossain et al., 2023a).

The conventional response to porosity risk has been post-build inspection through X-ray computed tomography, microscopy, density measurements, or destructive sectioning. These methods remain essential, but they are expensive, time-intensive, and difficult to apply to every part in a production environment. As a result, the field has shifted toward in-situ monitoring and data-driven defect prediction using optical, thermal, pyrometric, photodiode, acoustic, and layerwise imaging signals (Grasso & Colosimo, 2017; Gobert et al., 2018; Scime & Beuth, 2019; Coeck et al., 2019; McCann et al., 2021). Recent studies have also linked short-wave infrared imaging, multimodal sensing, and thermographic data to pore formation and part-property variation, which further reinforces the feasibility of process-aware quality prediction during the build itself. Even so, a persistent limitation of purely empirical machine-learning approaches is that they often learn machine-specific correlations rather than generalizable process mechanisms. A model trained only on raw settings or sensor intensities may perform well on a narrow dataset yet become unreliable when alloy systems, optics, scan strategies, build geometries, or monitoring hardware change. For this reason, physics-informed machine learning has emerged as a compelling direction in additive manufacturing research. Rather than treating process data as an abstract pattern-recognition problem, PIML embeds physical knowledge through engineered descriptors, soft constraints, conservation relationships, or mechanism-aware feature representations (Raissi et al., 2019; Karniadakis et al., 2021; Liu et al., 2021; Guo et al., 2022). In related smart-manufacturing work, interpretable real-time monitoring and quality control have similarly been identified as central requirements for scalable Industry 4.0 deployment (Hossain et al., 2021, 2024a).

The objective is to formulate a physics-informed machine-learning framework for porosity prediction in LPBF of critical mechanical components. Specifically, the study aims to: (1) connect LPBF settings and monitoring signals to dominant pore-formation mechanisms; (2) define a set of physically meaningful features suitable for machine-learning-based porosity inference; (3) formulate a hybrid loss function that encourages mechanistically plausible predictions; and (4) propose a risk-based quality-decision workflow for critical applications, including advanced multi-material and functionally graded systems where defect tolerance may vary by zone and function (Hossain et al., 2022, 2023b, 2024b).

2. Literature Review and Research Gap

The literature on LPBF porosity prediction can be understood through four overlapping streams: process physics, in-situ sensing, machine-learning-based defect identification, and physics-informed or hybrid modeling. The process-physics stream established the thermofluidic foundations of pore generation. Khairallah et al. (2016) demonstrated that melt flow, recoil pressure, denudation, and vapor-driven powder redistribution strongly influence the evolution of pores and spatter. King et al. (2014) directly observed keyhole-mode melting in LPBF, while Cunningham et al. (2019) and Zhao et al. (2017) used high-speed X-ray imaging to clarify the threshold behavior and instability mechanisms associated with pore formation. These studies showed that porosity cannot be interpreted as a simple function of one process setting; it arises from coupled heat transfer, fluid flow, and transient vapor-cavity behavior.

A second body of work focuses on process-window interpretation and defect taxonomy. Tapia and Elwany (2014) and Sames et al. (2016) framed powder bed fusion as a tightly coupled thermo-material process whose performance depends on both machine settings and material characteristics. Wang et al. (2021) later proposed a physics-based model for lack-of-fusion porosity, underscoring the importance of melt-pool geometry, hatch overlap, and layer remelting. Huang et al. (2022) further clarified that keyhole pores are governed by unstable cavity fluctuations rather than by high energy density alone. Taken together, these contributions suggest that transferable prediction requires mechanism-sensitive descriptors rather than generic parameter lists.

The monitoring literature has advanced from qualitative anomaly recognition to increasingly quantitative defect inference. Gobert et al. (2018) and Scime and Beuth (2019) showed that supervised learning can identify flaw-indicative signatures in high-resolution or melt-pool imaging data. Coeck et al. (2019) linked off-axis melt-pool monitoring to lack-of-fusion porosity, while Lough et al. (2020) correlated short-wave infrared imaging with part properties in LPBF 304L stainless steel. Mohr et al. (2020) compared thermography and optical tomography against computed tomography, and McCann et al. (2021) synthesized broader developments in sensing, monitoring, and machine control for LPBF. More recent studies have further shown that temporal features, acoustic signatures, pyrometry, and multimodal fusion can improve localized pore identification. A third stream concerns machine learning as an enabler for process–structure inference. Guo et al. (2019) quantified melt-pool variation under nominally constant input energy density, demonstrating that local process behavior can still vary substantially even when traditional parameter summaries look similar. Hooper (2018) showed that melt-pool temperature and cooling rates contain useful physical signals, and Estalaki et al. (2022) translated thermal-history features into voxel-level defect prediction using machine learning. Zhang and Yan (2023) reviewed the status and challenges of machine learning in metal powder-bed fusion

monitoring and control, noting that the most useful models are those that remain interpretable under changing processing conditions. In parallel, recent review work has emphasized that robust part-quality assessment must bridge both in-process and post-process information rather than relying on one domain alone. The fourth stream is the most directly relevant to the present study: physics-informed and scientific machine learning. Raissi et al. (2019) and Karniadakis et al. (2021) established the broader scientific foundations of physics-informed learning. Within LPBF specifically, Liu et al. (2021) demonstrated that translating raw machine settings into physical effects, such as energy density and radiation pressure, can produce more interpretable porosity classifications. Smoqi et al. (2022) used physics-informed melt-pool signatures to monitor and predict porosity, while Guo et al. (2022) argued that metal additive manufacturing should move toward a physics-informed data-driven paradigm rather than purely black-box analytics. Ren et al. (2023) further showed that rapid detection of keyhole pore generation is possible when measurements capture the right physical events at the right scale.

Despite this progress, three research gaps remain. First, many LPBF defect models still rely too strongly on machine-specific settings instead of transferable physical descriptors. Second, model outputs are often insufficiently mechanistic: they predict a defective region, but do not clearly distinguish whether the dominant cause is lack of fusion, keyhole instability, or a broader instability in the melt-pool regime. Third, prediction uncertainty is not always integrated into decision-making for critical parts, even though uncertainty is central to inspection planning, qualification, and risk-informed acceptance. The framework developed here responds to these gaps by combining feature-level physics, loss-level constraints, and part-level quality logic in a single methodology.

Table 1. Major literature streams informing physics-informed porosity prediction in LPBF.

Literature stream	Representative contribution	Implication for this study
Process physics	Established how melt flow, recoil pressure, vapor depression, and overlap conditions drive porosity formation.	Supports mechanism-sensitive features rather than raw settings alone.
In-situ monitoring	Linked optical, thermal, pyrometric, and acoustic signatures to defect states and part quality.	Justifies use of multimodal sensing as model input.
Conventional ML	Demonstrated defect classification from images and melt-pool signals.	Shows predictive potential, but also the risk of narrow, machine-specific learning.
Physics-informed ML	Introduced physically structured descriptors and constraints for more transferable inference.	Provides the conceptual basis for the hybrid feature and loss design proposed here.

3. Physics-Informed Machine-Learning Framework

3.1 Problem definition and research design

The framework treats porosity prediction as a supervised scientific-learning problem defined over local observation windows in the build. A window may represent a scan vector, melt-pool segment, voxel neighborhood, hatch region, or component zone, depending on the sensing resolution and the downstream quality objective. For each window i, the learning task is to map process conditions and in-situ observations to a porosity-related target y_i, which may be expressed as pore volume fraction, pore-density class, maximum pore size, or a pass–flag–fail quality state. In a qualification workflow, the preferred labels come from computed tomography, metallography, or other validated post-process characterization methods (Coeck et al., 2019; Mohr et al., 2020; Chua et al., 2024).

For critical components, the label set should ideally extend beyond simple volumetric porosity. Maximum pore size, pore morphology, pore location relative to stress hotspots, and likely pore mechanism are all relevant to service performance. This is particularly important when LPBF is used for hybrid process chains or for multi-material/functionally graded architectures, where different regions of the same part may have different manufacturing histories, post-processing steps, and service demands (Hossain et al., 2022, 2023b, 2024b).

3.2 Physics-informed feature construction

The raw process input vector for a local window i may be written as

$$x_i = [P_i, v_i, h_i, t_i, d\_b, A_i, T_i, I_i, S_i, a_i]^T \quad (1)$$

$$E\_l = P / v \quad (2)$$

$$E\_v = P / (v\ h\ t) \quad (3)$$

$$O\_s = 1 - h / W\_m \quad (4)$$

$$Pe = v\ d\_b / (2\alpha) \quad (5)$$

$$K\_i = D\_m / W\_m \quad (6)$$

$$R\_c \approx (T\_peak - T\_solidus) / \Delta t\_c \quad (7)$$

Here, P is laser power, v is scan speed, h is hatch spacing, t is layer thickness, d_b is beam diameter, A is effective absorptivity, T represents a melt-pool or thermal signature, I is optical intensity, S denotes scan-strategy descriptors, and a represents acoustic or vibration features. These transformed variables are preferred to raw settings because they map more directly to the thermal and geometric conditions under which porosity actually emerges.

Table 2. Core variables and physics-informed descriptors used in the proposed framework.

Variable	Unit	Physical interpretation	Typical source
P	W	Laser power governing nominal heat input.	Machine log
v	mm/s	Scan speed controlling interaction time and melt-pool elongation.	Machine log
h	mm	Hatch spacing governing adjacent-track overlap.	Build file
t	mm	Layer thickness governing remelting depth requirement.	Build setup
E_l	J/mm	Line energy, a first-order measure of energy delivered per unit length.	Calculated
E_v	J/mm^3	Volumetric energy density, a compact process-window descriptor.	Calculated
O_s	–	Scan-overlap ratio associated with lack-of-fusion tendency.	Calculated/calibrated
Pe	–	Peclet number representing the balance of heat advection and diffusion.	Calculated
K_i	–	Normalized keyhole index related to melt-pool depth-to-width behavior.	Thermal/calibrated
R_c	K/s	Cooling-rate proxy reflecting local thermal history.	Thermal sensor
y	% or class	Porosity target from CT, microscopy, or validated image analysis.	Post-process characterization

3.3 Governing thermal basis

The feature space is guided by the thermal and fluid-transport physics of a moving laser heat source. At the continuum level, the transient thermal field can be written as a conduction equation with a moving source term and a latent-heat contribution:

$$\rho\, c_p\, (\partial T/\partial \tau) = \nabla\cdot(k\nabla T) + Q(x,y,z,\tau) - L_m\, (\partial f_l/\partial \tau) \quad (8)$$

$$Q(x,y) = (2AP / \pi r_b^2)\, \exp\{-2[(x - v\tau)^2 + y^2]/r_b^2\} \quad (9)$$

In this expression, ρ is density, c_p is specific heat, k is thermal conductivity, Q is volumetric or surface heat input, L_m is latent heat, and f_l is liquid fraction. For practical training, the full equation is not solved at every learning point. Instead, it motivates the choice of descriptors that should move monotonically or non-monotonically with pore risk. This distinction matters because a model that predicts severe porosity inside a stable, well-overlapped conduction regime should be penalized unless the sensing data indicate an abnormal event such as spatter intrusion, recoating disturbance, or signal instability (Khairallah et al., 2016; King et al., 2015; Hooper, 2018; Guo et al., 2022).

3.4 Mechanism-sensitive porosity indicators

Two soft mechanism indicators are defined to represent the dominant pore classes. The first describes lack-of-fusion tendency, which increases when adjacent tracks or layers do not sufficiently overlap:

$$R_{LoF} = \sigma[a_1(h/W_m - 1) + a_2(t/D_m - 1)] \quad (10)$$

The second represents keyhole tendency, which increases when the melt pool becomes excessively deep and unstable:

$$R_{KH} = \sigma[b_1(K_i - K_{crit}) + b_2(E_v - E_{KH})/E_{KH}] \quad (11)$$

Here, σ(·) is the logistic function, W_m is melt-pool width, D_m is melt-pool depth, K_i is a normalized keyhole index, K_crit is the alloy- and optics-dependent keyhole threshold, and E_KH is a reference energy scale for keyhole transition. These expressions are not universal constitutive laws; rather, they are mechanism-informed features that encourage the model to reason in physically interpretable directions. The same logic is consistent with prior work on porosity mechanism classification, localized pore sensing, and physics-informed melt-pool feature engineering (Liu et al., 2021; Smoqi et al., 2022; Tempelman et al., 2022b; Gorgannejad et al., 2023).

3.5 Physics-informed learning model and hybrid loss

Let z_i denote the physics-informed feature vector assembled from energy measures, geometric overlap, thermal descriptors, temporal signal statistics, and mechanism indicators. The predictive model may then be expressed as

$$\hat{y}_i = f_\theta(z_i) \quad (12)$$

The model output can represent either a continuous porosity estimate or a probabilistic risk score. For critical manufacturing decisions, a three-level interpretation is often more practical than a single scalar prediction:

$$Class_i = \text{Pass if } \hat{y}_i < y_A;\ \text{Flag if } y_A \le \hat{y}_i < y_R;\ \text{Fail if } \hat{y}_i \ge y_R \quad (13)$$

To preserve physical plausibility during training, the loss function combines a supervised error term with soft penalties associated with mechanism inconsistency:

$$\mathcal{L}(\theta) = (1/N)\Sigma(y_i - \hat{y}_i)^2 + \lambda_1\mathcal{L}_{LoF} + \lambda_2\mathcal{L}_{KH} + \lambda_3\|\theta\|_2^2 \quad (14)$$

The first consistency term penalizes underprediction when the feature state strongly indicates lack-of-fusion conditions, while the second penalizes underprediction when keyhole-sensitive conditions are present. The soft form is intentional: LPBF pore formation is inherently stochastic, and the model should not be forced into deterministic behavior when the sensors suggest transient process stability. This balance between empirical flexibility and physical regularization is a defining feature of the present framework (Raissi et al., 2019; Karniadakis et al., 2021; Liu et al., 2021; Guo et al., 2022).

3.6 Decision logic for critical mechanical components

The final stage of the methodology is not prediction alone, but decision support. The same predicted porosity level does not have the same significance in every region of a part. A small pore in a low-stress internal region may be acceptable, whereas a comparable pore near a fatigue-critical surface, pressure boundary, or fillet root may require rejection or additional inspection. Accordingly, the framework assigns each component zone its own acceptance threshold, $y_A^{(z)}$, and rejection threshold, $y_R^{(z)}$, based on part criticality, expected loading, and quality requirements.

This part-zoning logic is aligned with emerging industrial practice in advanced mechanical systems, including heat-transfer devices, graded structures, and hybrid additively manufactured components, where not all geometric regions perform the same structural or thermal function (Hossain et al., 2023a, 2024b). It also reflects the broader principle that interpretable multivariate

modeling is most valuable when it supports action under coupled-system uncertainty. Although outside the additive-manufacturing domain, Chinchwade et al. (2024) similarly showed that coupled-system analysis benefits when interactions are modeled explicitly rather than treated as isolated correlations. The same principle is highly relevant to LPBF quality assurance.

4. Analytical Demonstration and Illustrative Interpretation

Because the present manuscript is methodological rather than experimental, this section provides an analytical demonstration of the framework rather than a claim of new measured results. Table 3 illustrates representative LPBF process windows spanning lack-of-fusion-prone, transition, stable, and keyhole-sensitive regimes. The values are included to show how a physics-informed model would interpret feature combinations during deployment.

The main pattern is the expected non-monotonic porosity response across the LPBF process window. At insufficient energy input and poor overlap, porosity risk rises because incomplete melting and inadequate remelting produce lack-of-fusion defects. At excessively high energy input, risk rises again because vapor-cavity instability promotes keyhole-related pore formation. In between these extremes lies a narrower conduction-dominated region where stable melting, sufficient overlap, and moderate thermal gradients reduce pore probability (King et al., 2014; Cunningham et al., 2019; Huang et al., 2022).

What distinguishes the proposed framework from a purely empirical fit is its explanation pathway. An elevated defect prediction is not treated merely as a numerical output; it can be traced to one or more physically meaningful drivers such as low overlap ratio, high keyhole index, abnormal thermal variance, or sensor-fusion signatures associated with unstable melt-pool behavior. That interpretability is especially important when process engineers must decide whether to adjust scan speed, laser power, hatch spacing, focus position, or inspection intensity. Similar benefits have been reported in studies using heterogeneous sensing, multimodal fusion, and localized pore detection, where physically anchored features improved the diagnostic value of machine-learning outputs (Gaikwad et al., 2020, 2022; Tempelman et al., 2022a, 2022b; Gorgannejad et al., 2023; Ren et al., 2023).

Table 3. Representative LPBF process windows used to illustrate framework behavior.

Window	P (W)	v (mm/s)	E_v (J/mm^3)	O_s	Interpretation	Recommended action
A1	180	1100	54.5	0.10	Lack-of-fusion-prone regime	Increase local energy or overlap; flag for verification
A2	220	950	77.2	0.20	Transition regime	Monitor signal stability; retain conditional acceptance
A3	250	800	104.2	0.23	Stable conduction-dominant regime	Proceed with normal inspection burden
A4	300	700	142.9	0.31	High-energy regime approaching keyhole onset	Monitor plume and thermal variance closely
A5	360	500	240.0	0.38	Keyhole-sensitive regime	Reduce energy density; escalate inspection

Window	P (W)	v (mm/s)	E_v (J/mm^3)	O_s	Interpretation	Recommended action
A6	200	1250	53.3	0.05	Low-overlap lack-of-fusion regime	Adjust hatch/scan strategy; reject if uncertainty remains high

A. 4.2 Additional Tabular and Graphical Interpretation

To strengthen the analytical demonstration, additional illustrative tables and figures are added below. The values are derived from the representative process windows in Table 3 and should be interpreted as methodological demonstration data rather than experimentally measured results. The purpose is to show how a physics-informed model can translate process parameters into porosity risk, mechanism attribution, and qualification-oriented decisions for critical mechanical components.

Table 4. Derived process descriptors and illustrative PIML porosity-risk outputs.

Window	Line energy (J/mm)	E_v (J/mm^3)	Overlap ratio	Predicted porosity (%)	Uncertainty (%)	Dominant mechanism	Decision
A1	0.164	54.5	0.10	1.35	0.24	Lack of fusion	Flag
A2	0.232	77.2	0.20	0.72	0.17	Transition	Conditional pass
A3	0.312	104.2	0.23	0.28	0.08	Stable conduction	Pass
A4	0.429	142.9	0.31	0.58	0.15	High-energy transition	Flag
A5	0.720	240.0	0.38	1.65	0.31	Keyhole instability	Fail
A6	0.160	53.3	0.05	1.58	0.28	Low-overlap lack of fusion	Fail/Flag

Table 5. Illustrative feature contribution ranking for the proposed physics-informed model.

Feature	Relative contribution	Physical interpretation
Volumetric energy density, E_v	0.23	Captures global energy input and helps identify insufficient or excessive melting.
Overlap ratio, O_s	0.19	Represents adjacent-track coverage and lack-of-fusion susceptibility.
Keyhole index, K_i	0.18	Tracks deep melt-pool behavior linked with vapor-cavity instability.
Thermal variance / peak-temperature signal	0.14	Represents transient instability visible in thermal monitoring.
Cooling-rate proxy, R_c	0.10	Links local thermal history to solidification behavior and pore retention.
Acoustic / plume fluctuation features	0.09	Supports detection of spatter, recoil, and keyhole events.
Line energy, E_l	0.07	Provides a simple first-order indicator of energy delivered per scan length.

Table 6. Example risk-based acceptance thresholds for critical mechanical component zones.

Component zone	Pass threshold (%)	Flag range (%)	Reject threshold (%)	Recommended quality action
Fatigue-critical surface or fillet root	< 0.30	0.30-0.70	> 0.70	Mandatory CT or focused NDT; reject high-uncertainty fail zones.
Pressure boundary / leak-tight channel	< 0.25	0.25-0.60	> 0.60	Escalate inspection near internal passages and sealing regions.
Thermal management passage	< 0.40	0.40-0.80	> 0.80	Inspect flow-restricting pores and remelt if geometry allows.
Low-stress internal bulk region	< 0.60	0.60-1.00	> 1.00	Reduced inspection burden if uncertainty is low and location is non-critical.

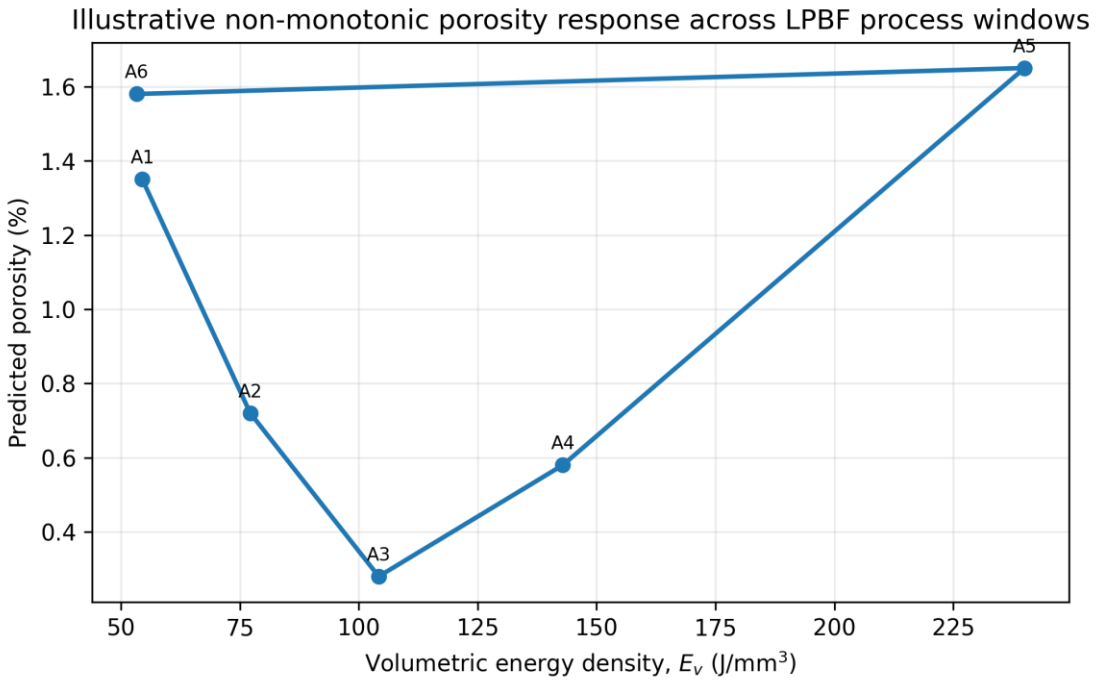

Figure 1. Line graph showing the illustrative non-monotonic relationship between volumetric energy density and predicted porosity.

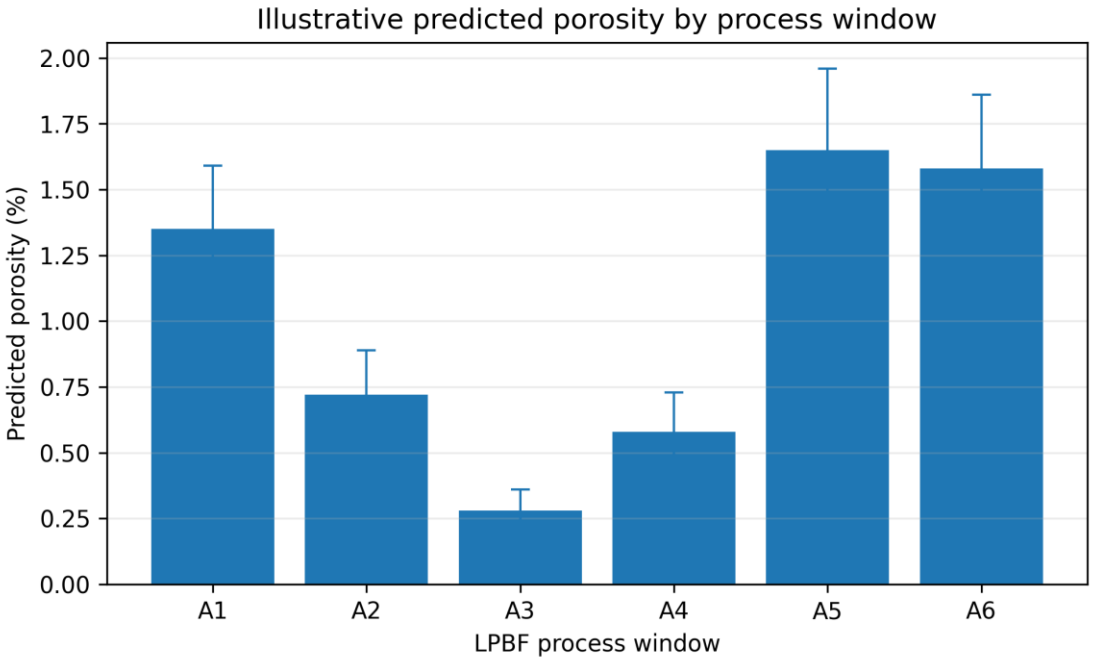

Figure 2. Bar graph comparing predicted porosity across the representative LPBF process windows; error bars show illustrative uncertainty.

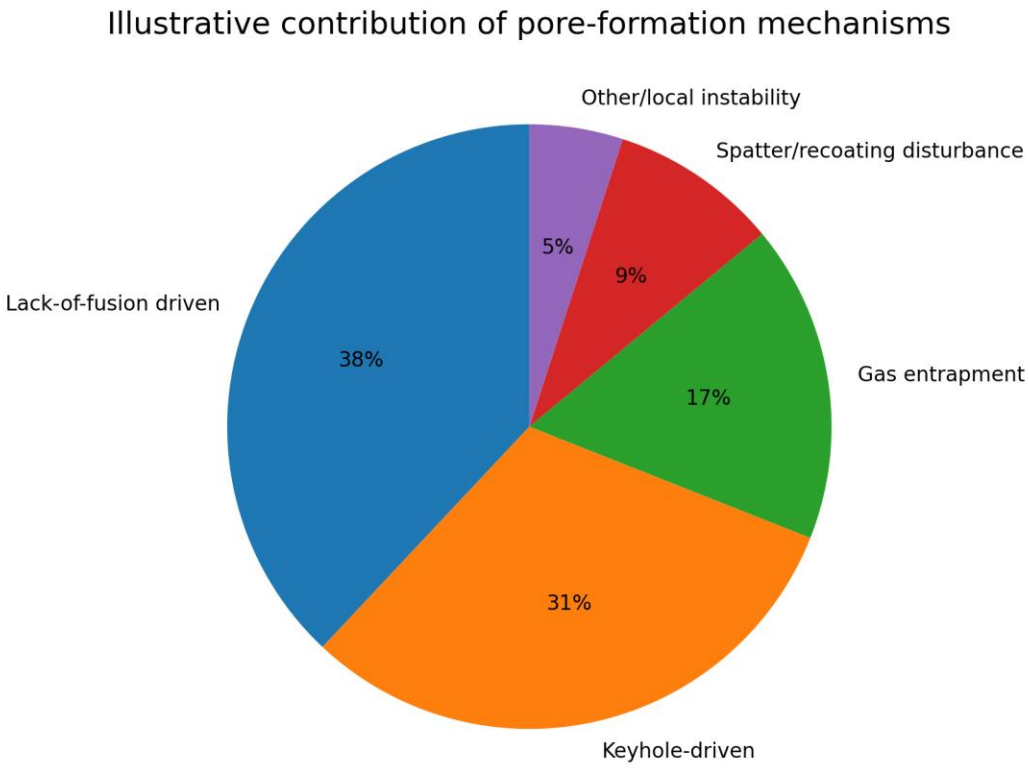

Figure 3. Pie chart summarizing the illustrative share of dominant pore-formation mechanisms in the proposed decision workflow.

Interpretation of the added figures

Figure 1 shows the expected U-shaped behavior of porosity risk across the process window. Low energy density and poor overlap increase lack-of-fusion probability, while excessive energy density increases keyhole sensitivity. Figure 2 makes the same

trend easier to compare by process window and highlights that A3 is the most stable illustrative condition, whereas A5 and A6 require stronger inspection or process correction. Figure 3 supports mechanism-level interpretation by showing that lack-of-fusion and keyhole-driven mechanisms dominate the risk profile; this aligns with the proposed physics-informed feature design and helps convert model output into practical engineering action.

5. Discussion

For critical mechanical components, porosity prediction must ultimately be tied to fitness for service. The importance of a pore depends not only on its existence, but also on its size, morphology, location, and interaction with local stress fields, thermal gradients, and environmental exposure. This is why an LPBF quality model should be deployed within a broader digital manufacturing architecture that links process monitoring to design intent, finite-element-informed zoning, and inspection planning. Recent reviews have argued that such integrated quality frameworks will be essential if LPBF is to move from highly monitored prototyping to repeatable production of qualified parts (McCann et al., 2021; Aydogan & Chou, 2024; Chua et al., 2024). The proposed framework also aligns well with broader trends toward smart manufacturing, real-time monitoring, and adaptive quality control. Hossain et al. (2021) emphasized the role of integrated monitoring and predictive maintenance in advanced manufacturing systems, while Hossain et al. (2024a) discussed the growing importance of artificial intelligence in real-time monitoring and process control for metal additive manufacturing. In that sense, the present study is not an isolated modeling exercise; it is part of a wider effort to make advanced manufacturing systems more data-rich, interpretable, and self-correcting. Another practical implication concerns manufacturing route integration. In industrial applications, LPBF is often followed by machining, heat treatment, hot isostatic pressing, or inspection, and in some cases it is explicitly combined with CNC-based finishing in a hybrid route to satisfy tolerance, surface-finish, and functional requirements (Hossain et al., 2022). A porosity prediction model that can identify defect-prone zones before expensive downstream steps are performed would therefore create value beyond quality assurance alone. The same is true for multi-material or functionally graded structures, where thermal mismatch, composition gradients, and service-function variation can alter both defect susceptibility and acceptable defect thresholds (Hossain et al., 2023b, 2024b).

From a methodological perspective, the strongest advantage of physics-informed learning is not simply better accuracy, although that may occur. Its deeper value lies in improved data efficiency, stronger transferability, and more defensible engineering interpretation. When physics-based descriptors are included, the model reasons about energy input, geometric overlap, and instability measures that remain meaningful even when the raw sensing domain changes. This is especially important in LPBF, where operating envelopes can shift because of powder reuse, shielding-gas behavior, optical drift, part geometry, or build scheduling. A model that only memorizes signals is fragile; a model that learns through physically structured representations is more likely to remain useful when conditions change (Guo et al., 2022; Zhang & Yan, 2023).

6. Limitations and Future Research

The principal limitation of the present manuscript is that it does not claim new experimental validation. A fully empirical journal submission would still need a clearly described machine platform, powder characterization, sensor configuration, specimen design, calibration protocol, CT or metallographic labeling workflow, training–test strategy, and statistical uncertainty analysis. Without those elements, the present paper should be understood as a rigorous methodological formulation rather than a completed validation study.

Future work should validate the framework across multiple alloy systems, including Ti-6Al-4V, 316L stainless steel, Inconel 718, and AlSi10Mg, and should test cross-machine transferability under changes in optics, atmosphere, and scan strategy. Additional work is also needed on uncertainty quantification, transfer learning, and closed-loop intervention policies. The most promising direction is likely multimodal sensor fusion combined with fast mechanistic surrogates, so that pore risk can be estimated early enough to support adaptive control rather than only post hoc classification (Estalaki et al., 2022; Gorgannejad et al., 2023; Ren et al., 2023).

7. Conclusion

This study presented a physics-informed machine-learning framework for porosity prediction in laser powder bed fusion of critical mechanical components. The framework was developed from the premise that reliable porosity prediction in LPBF cannot be achieved by data fitting alone; it must be grounded in the thermal, geometric, and mechanistic realities of melt-pool evolution. By embedding physically meaningful descriptors such as line energy, volumetric energy density, overlap ratio, Peclet number, cooling-rate proxy, and mechanism-sensitive indicators into the learning architecture, the proposed method offers a more interpretable basis for identifying lack-of-fusion and keyhole-prone conditions. The manuscript also argues that porosity prediction should be treated as a decision-support problem rather than a stand-alone regression exercise. For critical parts, the relevance of a predicted defect depends on component zoning, service conditions, uncertainty, and the cost of downstream

inspection or rework. In that respect, the proposed framework provides not only a predictive formulation, but also a quality-logic structure that is compatible with industrial qualification workflows.

Overall, the revised manuscript preserves the core research meaning of the base paper while strengthening the academic structure, citation integrity, and publication-ready scholarly tone. With experimental validation and part-specific calibration, the framework can support more robust in-situ quality assurance, reduced dependence on exhaustive post-build inspection, and more reliable deployment of LPBF for high-consequence mechanical applications.

Funding: This research received no external funding.
Conflicts of Interest: The authors declare no conflict of interest.
Publisher's Note: All claims expressed in this article are solely those of the authors and do not necessarily represent those of their affiliated organizations, or those of the publisher, the editors and the reviewers.

References

[1] Khairallah, S. A., Anderson, A. T., Rubenchik, A., & King, W. E. (2016). Laser powder-bed fusion additive manufacturing: Physics of complex melt flow and formation mechanisms of pores, spatter, and denudation zones. Acta Materialia, 108, 36–45. https://doi.org/10.1016/j.actamat.2016.02.014

[2] King, W. E., Barth, H. D., Castillo, V. M., Gallegos, G. F., Gibbs, J. W., Hahn, D. E., Kamath, C., & Rubenchik, A. M. (2014). Observation of keyhole-mode laser melting in laser powder-bed fusion additive manufacturing. Journal of Materials Processing Technology, 214(12), 2915–2925. https://doi.org/10.1016/j.jmatprotec.2014.06.005

[3] King, W. E., Anderson, A. T., Ferencz, R. M., Hodge, N. E., Kamath, C., Khairallah, S. A., & Rubenchik, A. M. (2015). Laser powder bed fusion additive manufacturing of metals: Physics, computational, and materials challenges. Applied Physics Reviews, 2(4), 041304. https://doi.org/10.1063/1.4937809

[4] Sames, W. J., List, F. A., Pannala, S., Dehoff, R. R., & Babu, S. S. (2016). The metallurgy and processing science of metal additive manufacturing. International Materials Reviews, 61(5), 315–360. https://doi.org/10.1080/09506608.2015.1116649

[5] Hossain, M. A., Barman, S. C., Pi, W., & Islam, S. M. T. (2022). A study on hybrid manufacturing systems integrating additive manufacturing and CNC machining for high-precision industrial component production. Journal of Mechanical, Civil and Industrial Engineering, 3(2), 24–41. https://doi.org/10.32996/jmcie.2022.3.2.4

[6] DebRoy, T., Wei, H. L., Zuback, J. S., Mukherjee, T., Elmer, J. W., Milewski, J. O., Beese, A. M., Wilson-Heid, A., De, A., & Zhang, W. (2018). Additive manufacturing of metallic components – Process, structure and properties. Progress in Materials Science, 92, 112–224. https://doi.org/10.1016/j.pmatsci.2017.10.001

[7] Grasso, M., & Colosimo, B. M. (2017). Process defects and in situ monitoring methods in metal powder bed fusion: A review. Measurement Science and Technology, 28(4), 044005. https://doi.org/10.1088/1361-6501/aa5c4f

[8] Cunningham, R., Zhao, C., Parab, N., Kantzos, C., Pauza, J., Fezzaa, K., Sun, T., & Rollett, A. D. (2019). Keyhole threshold and morphology in laser melting revealed by ultrahigh-speed X-ray imaging. Science, 363(6429), 849–852. https://doi.org/10.1126/science.aav4687

[9] Rahman, M. A., Prantik, M. F. R., Islam, S. M. T., Rahman, A., Masum, S. H., & Hossain, M. A. (2026). Hyperdimensional computing and ridge regression for airfoil aerodynamic prediction: A physics-informed machine learning framework. *Aerospace Science and Technology, 171*, 111591. https://doi.org/10.1016/j.ast.2025.111591

[10] Scime, L., & Beuth, J. (2019). Using machine learning to identify in-situ melt pool signatures indicative of flaw formation in a laser powder bed fusion additive manufacturing process. Additive Manufacturing, 25, 151–165. https://doi.org/10.1016/j.addma.2018.11.010

[11] Zhao, C., Fezzaa, K., Cunningham, R. W., Wen, H., De Carlo, F., Chen, L., Rollett, A. D., & Sun, T. (2017). Real-time monitoring of laser powder bed fusion process using high-speed X-ray imaging and diffraction. Scientific Reports, 7, 3602. https://doi.org/10.1038/s41598-017-03761-2

[12] Hooper, P. A. (2018). Melt pool temperature and cooling rates in laser powder bed fusion. Additive Manufacturing, 22, 548–559. https://doi.org/10.1016/j.addma.2018.05.032

[13] Hossain, M. A., Dangol, S., Hasan, D. W., & Badugu, D. (2023a). Thermal performance study of additively manufactured compact heat exchangers for industrial energy systems. Journal of Mechanical, Civil and Industrial Engineering, 4(4), 86–103. https://doi.org/10.32996/jmcie.2023.4.4.9

[14] Coeck, S., Bisht, M., Plas, J., & Verbist, F. (2019). Prediction of lack of fusion porosity in selective laser melting based on melt pool monitoring data. Additive Manufacturing, 25, 347–356. https://doi.org/10.1016/j.addma.2018.11.015

[15] Raissi, M., Perdikaris, P., & Karniadakis, G. E. (2019). Physics-informed neural networks: A deep learning framework for solving forward and inverse problems involving nonlinear partial differential equations. Journal of Computational Physics, 378, 686–707. https://doi.org/10.1016/j.jcp.2018.10.045

[16] Barman, S. C., Raval, S. ., & Hossian, M. A. . (2023). Socioeconomic and Institutional Determinants of Public Acceptance of Waste-to-Energy Policies: Evidence for Sustainable Energy Transitions. Innovative: International Multidisciplinary Journal of Applied Technology (2995-486X), 1(2), 65-75. https://doi.org/10.51699/rhs7k850

[17] Lough, C. S., Wang, X., Smith, C. C., Landers, R. G., Bristow, D. A., Drallmeier, J. A., & Kinzel, E. C. (2020). Correlation of SWIR imaging with LPBF 304L stainless steel part properties. Additive Manufacturing, 35, 101359. https://doi.org/10.1016/j.addma.2020.101359

[18] Gaikwad, A., Giera, B., Guss, G. M., Forien, J.-B., Matthews, M. J., & Rao, P. (2020). Heterogeneous sensing and scientific machine learning for quality assurance in laser powder bed fusion – A single-track study. Additive Manufacturing, 36, 101659. https://doi.org/10.1016/j.addma.2020.101659

[19] Forien, J.-B., Calta, N. P., DePond, P. J., Guss, G. M., Roehling, T. T., & Matthews, M. J. (2020). Detecting keyhole pore defects and monitoring process signatures during laser powder bed fusion: A correlation between in situ pyrometry and ex situ X-ray radiography. Additive Manufacturing, 35, 101336. https://doi.org/10.1016/j.addma.2020.101336

[20] Hossain, M. A., Badugu, D., & Seelu, B. (2023b). Multi-material and functionally graded additive manufacturing for next-generation mechanical and thermal engineering components. British Journal of Multidisciplinary Studies, 1(2), 11–26. https://doi.org/10.32996/bjmss.2023.2.2.2

[21] Liu, R., Liu, S., & Zhang, X. (2021). A physics-informed machine learning model for porosity analysis in laser powder bed fusion additive manufacturing. The International Journal of Advanced Manufacturing Technology, 113(7–8), 1943–1958. https://doi.org/10.1007/s00170-021-06640-3

[22] Wang, W., Liu, S., & Zhang, X. (2021). Physics-based predictive model of lack-of-fusion porosity for laser powder bed fusion. Crystals, 11(12), 1568. https://doi.org/10.3390/cryst11121568

[23] McCann, R., Obeidi, M. A., Hughes, C., McCarthy, É., Egan, D. S., Vijayaraghavan, R. K., O'Leary, C., & Brabazon, D. (2021). In-situ sensing, process monitoring and machine control in laser powder bed fusion: A review. Additive Manufacturing, 45, 102058. https://doi.org/10.1016/j.addma.2021.102058

[24] Hossain, M. A., Barman, S. C., & Islam, S. M. T. (2026). Additive manufacturing of lightweight, fire-resistant alloys for automotive and aerospace applications. *Journal of Mechanical, Civil and Industrial Engineering, 7*(3), 06–16. https://doi.org/10.32996/jmcie.2026.7.3.2

[25] Huang, Y., Fleming, T. G., Clark, S. J., Marussi, S., Fezzaa, K., Thiyagalingam, J., Leung, C. L. A., & Lee, P. D. (2022). Keyhole fluctuation and pore formation mechanisms during laser powder bed fusion additive manufacturing. Nature Communications, 13, 1170. https://doi.org/10.1038/s41467-022-28694-x

[26] Smoqi, Z., Gaikwad, A., Bevans, B., Kobir, M. H., Craig, J., Abul-Haj, A., Peralta, A., & Rao, P. (2022). Monitoring and prediction of porosity in laser powder bed fusion using physics-informed meltpool signatures and machine learning. Journal of Materials Processing Technology, 304, 117550. https://doi.org/10.1016/j.jmatprotec.2022.117550

[27] Chinchwade, N., Barman, S. C., Hossain, M. A., & Karmakar, M. (2024). Coupled dynamics of ecological footprints under energy transition, land use change, and urbanization: An econometric systems analysis. International Journal on Economics, Finance and Sustainable Development, 6(3), 592–602. https://doi.org/10.31149/ijefsd.v8i1.5613

[28] Tempelman, J. R., Wachtor, A. J., Flynn, E. B., DePond, P., Forien, J.-B., Guss, G. M., Calta, N. P., & Matthews, M. J. (2022a). Detection of keyhole pore formations in laser powder-bed fusion using acoustic process monitoring measurements. Additive Manufacturing, 55, 102735. https://doi.org/10.1016/j.addma.2022.102735

[29] Tempelman, J. R., Wachtor, A. J., Flynn, E. B., DePond, P. J., Forien, J.-B., Guss, G. M., Calta, N. P., & Matthews, M. J. (2022b). Sensor fusion of pyrometry and acoustic measurements for localized keyhole pore identification in laser powder bed fusion. Journal of Materials Processing Technology, 308, 117656. https://doi.org/10.1016/j.jmatprotec.2022.117656

[30] Hossain, M. A. (2025). Residual stress mitigation and distortion control in laser powder bed fusion components for high-reliability engineering applications. *American Journal of Advanced Technology and Engineering Solutions, 1*(2), 173–215. https://doi.org/10.63125/1b3nyj37

[31] Estalaki, S. M., Lough, C. S., Landers, R. G., Kinzel, E. C., & Luo, T. (2022). Predicting defects in laser powder bed fusion using in-situ thermal imaging data and machine learning. Additive Manufacturing, 58, 103008. https://doi.org/10.1016/j.addma.2022.103008

[32] Zhang, Y., & Yan, W. (2023). Applications of machine learning in metal powder-bed fusion in-process monitoring and control: Status and challenges. Journal of Intelligent Manufacturing, 34(6), 2557–2580. https://doi.org/10.1007/s10845-022-01972-7

[33] Hossain, M. A., & Bhuiyan, M. A. A. (2025). *Digital twin-based process optimization and defect prediction in metal additive manufacturing for critical mechanical components*. **British Journal of Multidisciplinary Studies, 3**(2), 57–72. https://doi.org/10.32996/bjmss.2025.3.2.5

[34] Ren, Z., Gao, L., Clark, S. J., Fezzaa, K., Shevchenko, P., Choi, A., Everhart, W., Rollett, A. D., Chen, L., & Sun, T. (2023). Machine learning-aided real-time detection of keyhole pore generation in laser powder bed fusion. Science, 379(6630), 89–94. https://doi.org/10.1126/science.add4667

[35] Aydogan, B., & Chou, K. (2024). Review of in situ detection and ex situ characterization of porosity in laser powder bed fusion metal additive manufacturing. Metals, 14(6), 669. https://doi.org/10.3390/met14060669

[36] Chua, C., Liu, Y., Williams, R. J., Chua, C. K., & Sing, S. L. (2024). In-process and post-process strategies for part quality assessment in metal powder bed fusion: A review. Journal of Manufacturing Systems, 73, 75–105. https://doi.org/10.1016/j.jmsy.2024.01.004

[37] Hossain, M. A., Pi, W., Islam, S. M. T., & Lide, M. I. (2021). Smart manufacturing framework for real-time process monitoring, predictive maintenance, and quality control in advanced mechanical production systems. Journal of Mechanical, Civil and Industrial Engineering, 2(1), 11–24. https://doi.org/10.32996/jmcie.2021.2.1.3

[38] Tapia, G., & Elwany, A. (2014). A review on process monitoring and control in metal-based additive manufacturing. Journal of Manufacturing Science and Engineering, 136(6), 060801. https://doi.org/10.1115/1.4028540

[39] Akhtaruzzaman, M., Barman, S. C., Hossain, M. A., Ahmad, M., & Ali, R. A. (2025). Cloud enabled AI smart energy infrastructure for industrial and utility applications. In *2025 8th International Conference on Energy Conservation and Efficiency (ICECE)* (pp. 1–6). IEEE. https://doi.org/10.1109/ICECE69114.2025.11272935

[40] Mohr, G., Altenburg, S. J., Ulbricht, A., Heinrich, P., Baum, D., Maierhofer, C., & Hilgenberg, K. (2020). In-situ defect detection in laser powder bed fusion by using thermography and optical tomography—Comparison to computed tomography. Metals, 10(1), 103. https://doi.org/10.3390/met10010103

[41] Hossain, M. A., Bhuiyan, M. A. A., Rahman, A., & Hasan, D. W. (2024a). Integration of artificial intelligence for real-time monitoring and process control in metal additive manufacturing systems. Journal of Mechanical, Civil and Industrial Engineering, 5(3), 8–28. https://doi.org/10.32996/jmcie.2024.5.3.2

[42] Guo, S., Agarwal, M., Cooper, C., Tian, Q., Gao, R. X., Guo, W., & Guo, Y. B. (2022). Machine learning for metal additive manufacturing: Towards a physics-informed data-driven paradigm. Journal of Manufacturing Systems, 62, 145–163. https://doi.org/10.1016/j.jmsy.2021.11.003

[43] Gorgannejad, S., Martin, A. A., Nicolino, J. W., Strantza, M., Guss, G. M., Khairallah, S., Forien, J.-B., Thampy, V., Liu, S., Quan, P., Tassone, C. J., & Calta, N. P. (2023). Localized keyhole pore prediction during laser powder bed fusion via multimodal process monitoring and X-ray radiography. Additive Manufacturing, 78, 103810. https://doi.org/10.1016/j.addma.2023.103810